11/21/77

FERMILAB-PUB-78-158-E BNL-23088-R
OG-372

Submitted to
Physics Letters B

Angular Dependence of High Transverse Momentum Inclusive π^0 Production in $\pi^{\pm}p$ and pp Interactions

G. Donaldson, H.A. Gordon, K.-W. Lai, and I. Stumer
Brookhaven National Laboratory, Upton, New York 11973

and

A.V. Barnes, D.J. Mellema,[a] A.V. Tollestrup,[b] and R.L. Walker
California Institute of Technology, Pasadena, California 91125

and

O.I. Dahl, R.A. Johnson,[c] A. Ogawa, M. Pripstein, and S. Shannon
Lawrence Berkeley Laboratory, Berkeley, California 94720

We have measured the inclusive π^0 production at high transverse momentum from both pion and proton beams at 100 and 200 GeV/c. Salient characteristics are a wide plateau in the c.m. angular distribution and evidence for scaling in both πp and pp interactions. The $\pi^{\pm}p \to \pi^0X$ cross sections fall less steeply with $x_\parallel = (p_\parallel/p_{max})$ c.m., and peak at $x_\parallel = 0.14$, in contrast to the $pp \to \pi^0X$ cross sections, which peak at $x_\parallel = 0$.

(a) Present address: Hughes Aircraft Company, Culver City, CA 90230

(b) Present address: Fermilab, Batavia, IL 60510

(c) Present address: Brookhaven National Laboratory, Upton, NY 11973

The observation of particles produced at large transverse momentum ($p_\perp$) has provided considerable insight into the fundamental interaction between the constituents of the incident hadrons. Not only theoretical, but also experimental effort has concentrated on proton-proton interactions in the central region [around 90^o in the center of mass (c.m.)]. Progress in understanding may be made by extending the data over larger angular regions, and by varying the constituent composition of the incident beam. Toward this end, we present the first comparison of inclusive π^o production from $\pi^\pm$ and p beams in a broad kinematic region. We find a significant difference in the $x_{\parallel} = (p_{\parallel}/p_{max})_{c.m.}$ distribution of π^os produced by pions compared to that produced by protons. New data from forward angles enable us to probe the difference in the momentum distribution of constituents in the pion and proton.

The experiment was conducted in the M2 beam at FNAL, and the apparatus and a subset of the data limited to the 90^o region have been described elsewhere.[1] The experimental apparatus consisted of two independent Cerenkov counters for tagging individual beam particles, a liquid hydrogen target, and a photon detector.[2]

The photon detector consisted of alternating layers of scintillator and lead sheets. The layers of scintillator were divided horizontally and vertically into 70 long narrow rods (73.5 x 1.05 cm). Eight layers were coupled together to integrate the shower development through 19 radiation lengths of lead, and the pulse height distributions in these counters were proportional to the energy deposited by photons hitting the detector. The position and energy of showers found in the detector allowed the mass of the parent particle to be reconstructed. The mass spectra of photon pairs (corrected for geometrical acceptance and with empty target background subtracted) were divided into course bins in $P_\perp$ and $x_{\parallel}$. The spatial resolution (± 1 mm), energy resolution ($\Delta E/E$ FWHM = $.20/\sqrt{E(\mathrm{GeV})}$) and target length (60 cm) contribute to an overall resolution of $\Delta m^2/m^2 = 12\%$. The π^o signal was extracted by fitting a gaussian signal plus a linear background to each mass distribution. The background has a magnitude $\sim 10\%$ of the π^o signal and is composed of pairs of unrelated photons and hadronic showers. The measurements presented herein cover the angular region $15^o - 115^o$ in the c.m. for $\pi^\pm$ and p beams at 100 and 200 GeV/c, and they also include $\pi^\pm$ and p forward angle data ($2^o - 20^o$) at 100 GeV/c, and 300 GeV/c pp data in the c.m. region $60^o - 110^o$.

Figure 1 shows the invariant cross section[3] for particular bins of $p_\perp$ plotted against $x_\parallel$. Several features are apparent visually: the pp cross sections appear to reach a maximum at $x_\parallel = 0$ as required by symmetry, and fall rapidly with increasing $x_\parallel$. In contrast, the $\pi^- p$ cross sections[4] appear to reach a maximum at $x_\parallel > 0$, and vary much less rapidly with increasing $x_\parallel$. For example, at 100 GeV/c for $2.0 < p_\perp < 2.4$ GeV/c the $\pi^- p$ and pp cross sections are nearly equal at $x_\parallel = 0$ but by $x_\parallel = 0.7$ the $\pi^- p$ cross section exceeds that of the pp by an order of magnitude. Data at much lower $p_\perp$ have indicated such a shift in $\pi^\pm p$ inclusive reactions[5]; however, this is the first observation at high transverse momentum. As another way of visualizing the same data, Figure 2 shows the invariant cross sections versus $\theta_{c.m.}$.[6] The central plateau for inclusive production is quite striking: the πp cross sections are roughly flat from 90^o to $\sim 30^o$ in the c.m. As has been measured at the ISR,[7] the pp cross sections are also flat, but in a more limited region $50^o \leq \theta_{c.m.} \leq 90^o$.

All the data points at all available energies for a particular beam type (with $x_\parallel < 0.8$) have been fit[8] to an empirical form $E\, d\sigma/dp^3 = A(1-x_D)^F/(p_\perp{}^2+m^2)^N$ where $x_D = \left\{x_\perp{}^2+(x_\parallel-x_o)^2\right\}^{1/2}$ and $x_\perp = (p_\perp/p_{max})$c.m. Here x_o is the value of $x_\parallel$ at the peak in the $x_\parallel$ distribution and hence represents the displacement (as in the πp data) of the peak position from $x_{\parallel} = 0$. For $x_o = 0$ (as for the pp data) x_D is then the usual radial variable $x_R = (x_{\perp}^2 + x_{\parallel}^2)^{1/2}$. The parameters A, m^2, F, N, and x_o are determined from the fit, and the smooth curves shown in Figures 1 and 2 display the parameterization using the best-fit values given in Table I. It is visually apparent that this simple form is qualitatively able to describe data within an extensive region of the Peyrou plot.

Several features of the data are evident from this fit: 1) the $p_{\perp}$ dependence at fixed x_D is virtually identical for πp and pp interactions. [$(p_{\perp}^2+m^2)^{-N}$ where $N_p = 4.9$ and $N_{\pi} = 5.0$].[10] 2) The πp interactions have an $x_{\parallel}$ dependence which peaks at $x_{\parallel} = 0.14$ while the pp interactions are symmetric about $x_{\parallel} = 0$. 3) The $\pi^- p$ cross sections scale as a function of x_D independent of $\theta_{c.m.}$ and s as shown in Figure 3 where the $(p_{\perp}^2+m^2)^{-N}$ dependence is multiplied out. Although not shown, the pp cross sections scale as a function of x_R. Since $x_R \neq x_D$, if $x_o \neq 0$, x_D scaling in πp interactions implies only approximate radial scaling. 4) Our determination of $(1-x_R)^{4.4}$ for the pp data depends more on the angular dependence of the data rather than its energy dependence. This value of F agrees with that found by Carey et al.[11] in a similar kinematic region. The $pp \to \pi^o X$ cross sections measured in this experiment are consistent with the average of the π^+ and π^- results in $pp \to \pi^{\pm} X$ at FNAL over a larger range of $P_{\perp}$ at 90^o.[12] However, the energy dependence of the $pp \to \pi^{\pm} X$ cross sections at fixed $P_{\perp}$ requires a $(1-x_{\perp})^9$ form. A generalization of this to $(1-x_R)^9$ would be too steep to accommodate the angular behavior of our data.

Some of these features of the data can be understood in the context of hard scattering models.[13-15] The value of N primarily arises from the scattering amplitude of the constituent-constituent scattering, thus the similarity between N_p and N_{π} strongly suggests that the same constituent scattering is involved in both reactions. The fact that the maximum of the πp cross section occurs for

$x_{\parallel} \to 0$ can be understood in that a quark in the pion has on the average a higher momentum than a quark in a proton, and therefore the quark-quark system is not at rest in the πp c.m. system.[16] The $(1-x_D)$ dependence primarily arises from the momentum distribution of constituents within the incoming particles. The $(1-x_D)^{3.1}$ for the $\pi^- p$ interactions is substantially less steep than $(1-x_D)^{4.4}$ for pp interactions, which can be interpreted to mean that the structure function for pions is flatter than protons.

In summary, there are several conclusions to be drawn from this analysis: a) Both πp and pp interactions scale as a function of a dimensionless variable; b) The same constituent scattering prevails in both πp and pp interactions; c) On the average, constituents of the pion have a higher momentum than those in the proton.

We wish to acknowledge a helpful conversation with R.B. Palmer, and the continuing support of R. Kenney. This research supported by the U.S. Department of Energy under contract No. EY-76-C-02-0016.

REFERENCES AND FOOTNOTES

1. G. Donaldson, et al., Phys. Rev. Lett. 36, (1976) 1110.
2. For details of the photon detector, see O. I. Dahl, et al., Phys. Rev. Lett. 37, (1976) 80.
3. Space limitations prohibit complete presentation of the data. BNL-~~#50726~~ 23844 contains the data in a tabular form.
4. In this experiment all $\pi^- p \to \pi^\circ X$ data are consistent with $\pi^+ p \to \pi^\circ X$, and only the (more complete) $\pi^- p$ data are presented herein.
5. P. Bosetti, et al., Nucl. Phys. B54, (1973) 141.
6. The values and extent of $\theta_{c.m.}$ for which these data are plotted correspond to the center and width of a $\Delta p_\perp$, $\Delta x_\parallel$ bin; i.e. the data are not rebinned.
7. K. Eggert, et al., Nucl. Phys. B98, (1975) 49.
8. Including also pp data at 300 GeV/c in the 90° cm region. Note that data for $x_\parallel \gtrsim 0.8$ is not included in the fit. The parametrization is integrated over $p_\perp$ and $x_\parallel$ and then compared to the data in each bin.
9. Two effects occur if one parameterizes the πp cross sections without an $x_\parallel$ offset: the band of data points shown in Figure 3 becomes substantially more scattered, and the χ^2 of the parameterization increases by a factor of ~ 1.5.
10. Although we do not measure $p_\perp^{-8}$ as has been seen in other experiments at FNAL, and the ISR, we note that in the limited interval $1 < p_\perp < 4$ GeV/c, it is quite difficult to distinguish $p_\perp^{-8}$ from $(p_\perp^2 + m^2)^{-5}$; thus experiments with data extending to higher ranges of $p_\perp$ have a better determination of the $p_\perp$ falloff. Alternatively, this may be a transition region in which the deviation from low $p_\perp$ exponential falloff has not been completely established.

11. D. C. Carey, et al., Phys. Rev. Lett. 33, (1974) 327.

12. D. Antreasyan, et al., Phys. Rev. Lett. 38, (1977) 112.

13. R. Blankenbecler, S. J. Brodsky and J. Gunion, Phys. Rev. D12, (1975) 3469.

14. R. D. Field and R. P. Feynmann, Phys. Rev. D15, (1977) 2590.

15. E. Fishbach and G. W. Look, Phys. Rev. D15, (1977) 2576.

16. S. Fredricksson, Phys. Rev. Lett. 37, (1976) 1373.
Note that a similar argument pertains to the forward peaking of ψ production in the $\pi^- p$ reactions. M. J. Corden, et al., Phys. Lett. 68B, (1977) 96.

TABLE I. Values obtained for least squares-fit to the form $E\frac{d\sigma}{dp^3} = A\frac{(1-x_D)^F}{(p_\perp^2+m^2)^N}$, where $x_D = (x_\perp^2 + (x_{\|} - x_o)^2)^{1/2}$ (Fits for $x_{\|} < 0.8$)

Beam Particle (Beam momenta fit) GeV	A ($\times 10^{-25}$ cm^2/GeV^2)	F	x_o	N	m^2 $(GeV/c^2)^2$	χ^2/DOF
pp (100,200,300)	0.122±0.015	4.42±0.05	0.02±0.01	4.90±0.06	0.81±0.04	306/142
π^-p (100,200)	0.113±0.015	3.13±0.10	0.14±0.01	5.06±0.06	0.97±0.04	271/132
π^+p (100,200)	0.102±0.015	3.29±0.10	0.14±0.01	5.00±0.07	0.95±0.04	325/130

FIGURE CAPTIONS

Fig. 1. The invariant cross section for π^o production versus $x_{\parallel}$ for several reactions: (a) $\pi^- p$ at 100 GeV/c; (b) pp at 100 GeV/c; (c) $\pi^- p$ at 200 GeV/c; (d) pp at 200 GeV/c. For display purposes, the cross sections in alternate $p_{\perp}$ intervals are labelled. Smooth curves indicate the parameterization described in the text.

Fig. 2. The invariant cross section versus $\theta_{c.m.}$ for $\pi^- p \to \pi^o + X$ at 100 GeV/c. Alternating $p_{\perp}$ intervals are labelled and are denoted by open and closed symbols. These points are plotted at the $\theta_{c.m.}$ corresponding to the bin centers of $p_{\perp}$, $x_{\parallel}$ bins shown in Fig. 1(a). The smooth curves display the parameterization described in the text.

Fig. 3. The invariant cross section multiplied by $(p_{\perp}^2 + m^2)^N$ for $\pi^- p$ interactions at 100 and 200 GeV/c, where the values used are $m^2 = 0.97$ and $N = 5.06$. Data in three angular regions (90°, 30°, 10°) fall on the same band. The smooth curve displays the parameterization, and demonstrates that this quantity no longer depends on $\theta_{c.m.}$ or s.

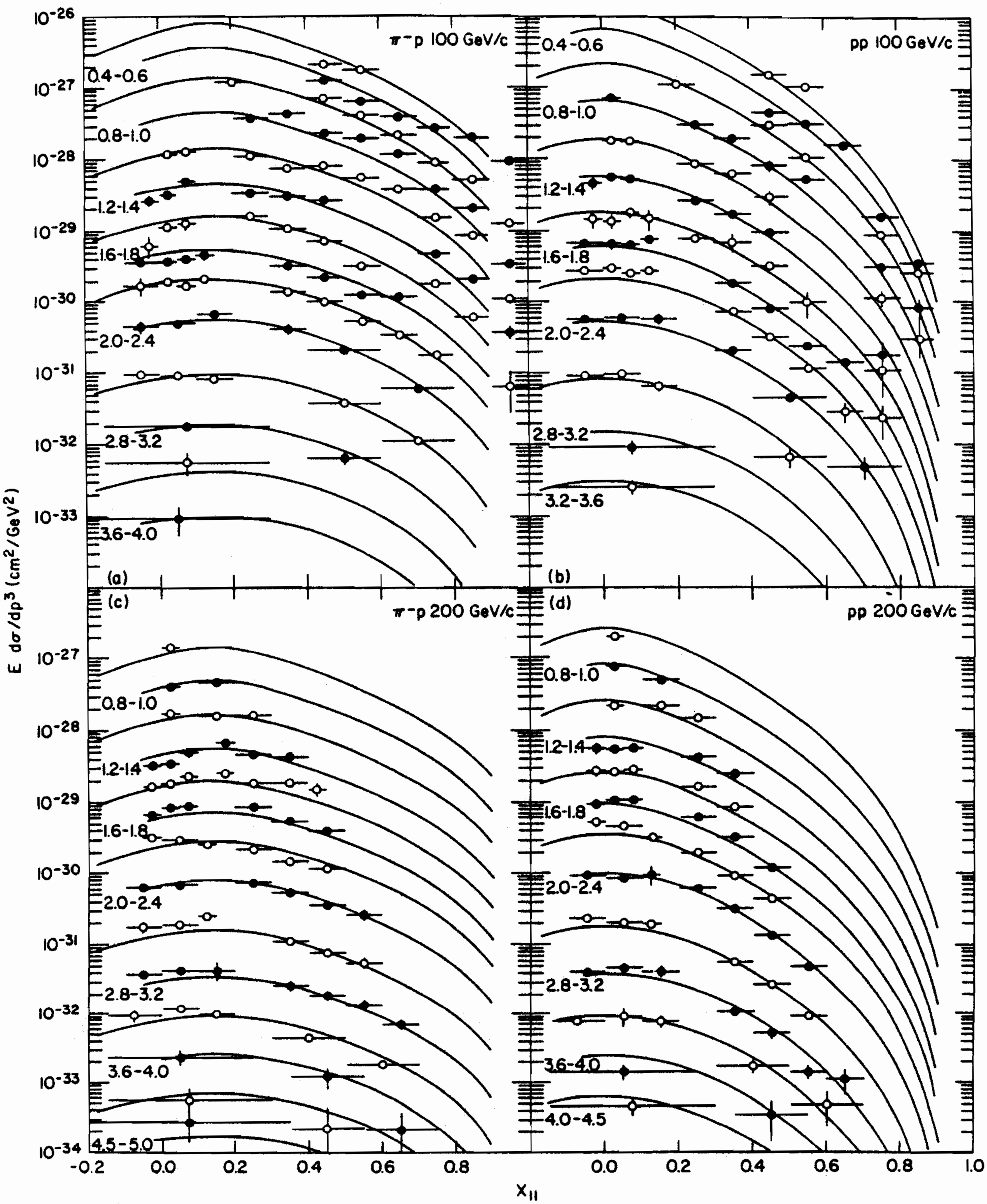

π⁻p 100 GeV/c
pp 100 GeV/c
π⁻p 200 GeV/c
pp 200 GeV/c
(a)
(b)
(c)
(d)
0.4-0.6
0.8-1.0
1.2-1.4
1.6-1.8
2.0-2.4
2.8-3.2
3.2-3.6
3.6-4.0
4.0-4.5
4.5-5.0
E dσ/dp³ (cm²/GeV²)
x∥
-0.2
0.0
0.2
0.4
0.6
0.8
1.0
10⁻²⁶
10⁻²⁷
10⁻²⁸
10⁻²⁹
10⁻³⁰
10⁻³¹
10⁻³²
10⁻³³
10⁻³⁴

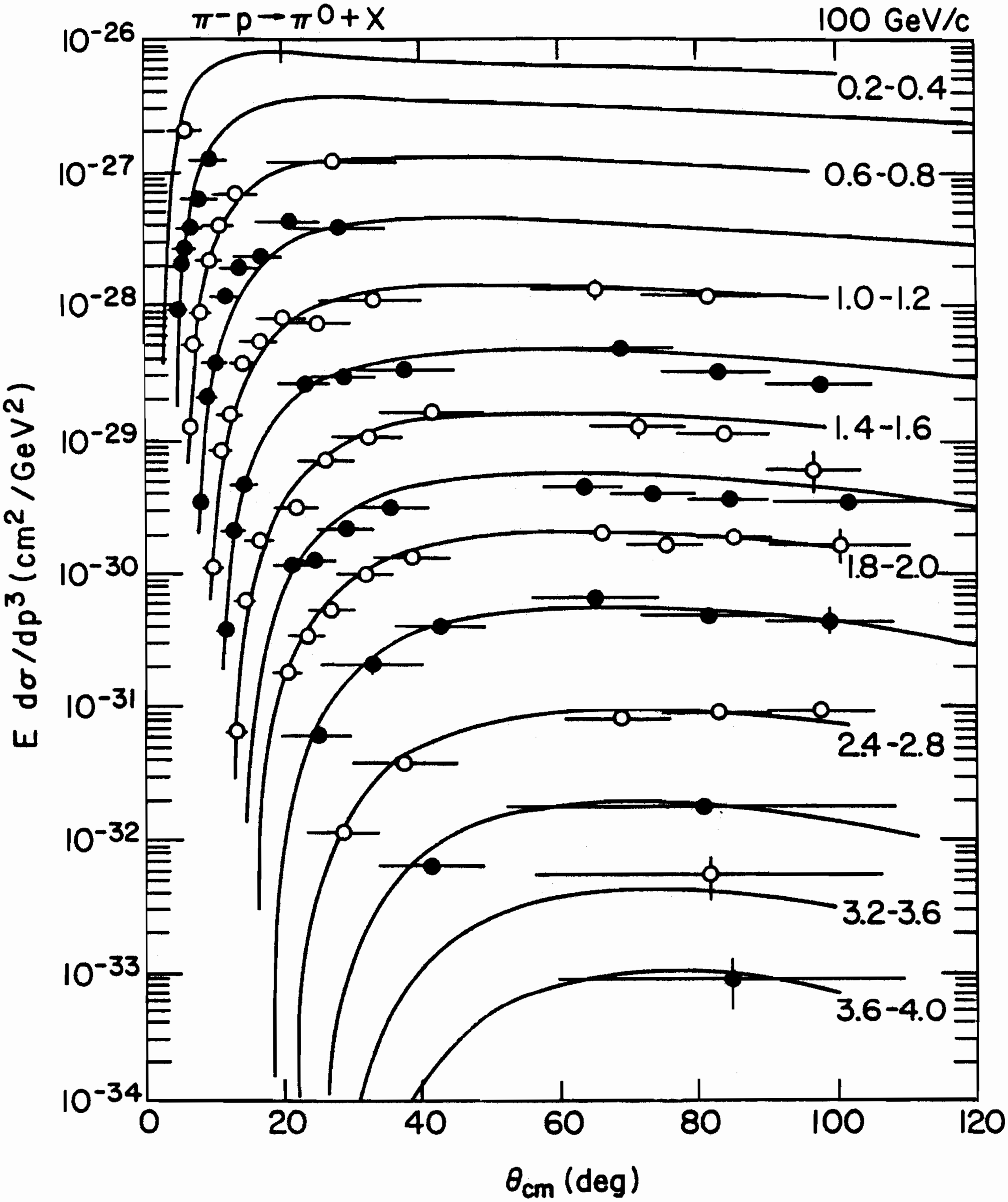

π⁻p → π⁰ + X
100 GeV/c
0.2-0.4
0.6-0.8
1.0-1.2
1.4-1.6
1.8-2.0
2.4-2.8
3.2-3.6
3.6-4.0
E dσ/dp³ (cm²/GeV²)
θcm (deg)

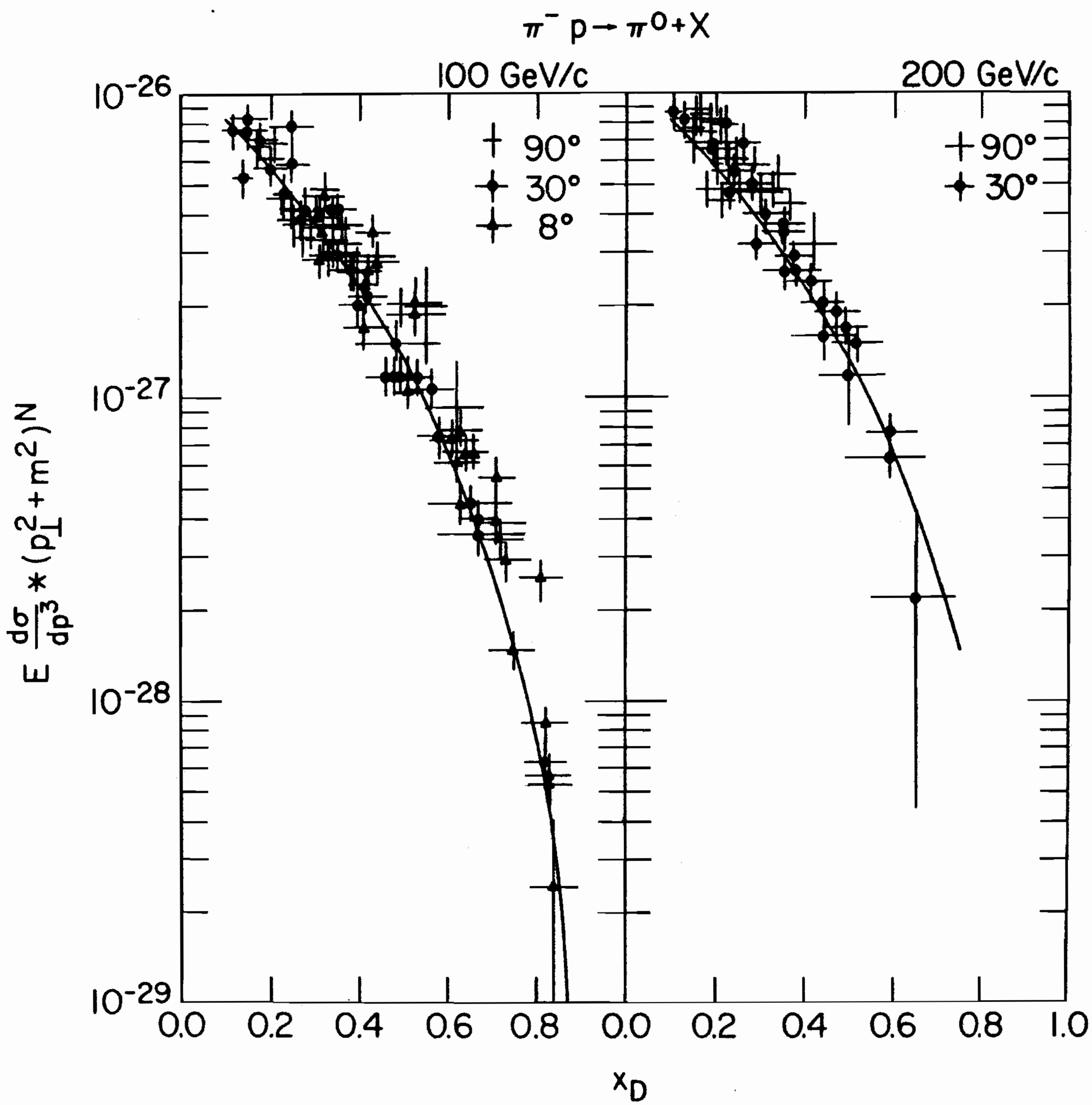

$\pi^- p \to \pi^0 + X$
100 GeV/c
200 GeV/c
90°
30°
8°
90°
30°
10^{-26}
10^{-27}
10^{-28}
10^{-29}
$E \frac{d\sigma}{dp^3} * (p_\perp^2 + m^2)^N$
0.0 0.2 0.4 0.6 0.8 0.0 0.2 0.4 0.6 0.8 1.0
x_D